JEM Journal of Experimental Medicine

ARTICLE

Somatic activating mutations in *PIK3CA* cause generalized lymphatic anomaly

Lara Rodriguez-Laguna[1], Noelia Agra[1], Kristina Ibañez[2], Gloria Oliva-Molina[1], Gema Gordo[1], Noor Khurana[3], Devon Hominick[3], María Beato[4], Isabel Colmenero[5], Gonzalo Herranz[1], Juan M. Torres Canizalez[6], Rebeca Rodríguez Pena[6], Elena Vallespín[7,8], Rubén Martín-Arenas[7], Ángela del Pozo[2], Cristina Villaverde[8,9], Ana Bustamante[8,9], Carmen Ayuso[8,9], Pablo Lapunzina[8,10], Juan C. Lopez-Gutierrez[11], Michael T. Dellinger[3,12], and Victor Martinez-Glez[1,8,10]

Generalized lymphatic anomaly (GLA) is a vascular disorder characterized by diffuse or multifocal lymphatic malformations (LMs). The etiology of GLA is poorly understood. We identified four distinct somatic *PIK3CA* variants (Glu542Lys, Gln546Lys, His1047Arg, and His1047Leu) in tissue samples from five out of nine patients with GLA. These same *PIK3CA* variants occur in *PIK3CA*-related overgrowth spectrum and cause hyperactivation of the PI3K–AKT–mTOR pathway. We found that the mTOR inhibitor, rapamycin, prevented lymphatic hyperplasia and dysfunction in mice that expressed an active form of *PIK3CA* (His1047Arg) in their lymphatics. We also found that rapamycin reduced pain in patients with GLA. In conclusion, we report that somatic activating *PIK3CA* mutations can cause GLA, and we provide preclinical and clinical evidence to support the use of rapamycin for the treatment of this disabling and deadly disease.

Introduction

Generalized lymphatic anomaly (GLA), formerly known as lymphangiomatosis, is a sporadic disorder characterized by diffuse or multifocal lymphatic malformations (LMs; Lala et al., 2013). Because of the low incidence of the disease, the literature on GLA is confined to case reports and several small series. These reports have revealed that GLA typically presents at birth or in children and young adults (Lala et al., 2013; Ozeki et al., 2016). Patients with GLA frequently display lymphatic abnormalities in their skin, soft tissues, and abdominal and thoracic viscera. These lymphatic abnormalities can cause pericardial, pleural, or peritoneal effusions, which can have lethal consequences (Lala et al., 2013; Trenor and Chaudry, 2014). Strikingly, patients with GLA can also have lymphatic vessels in their bones (Lala et al., 2013). The presence of bone lymphatics is associated with the loss of medullary bone, pain, and impaired mobility (Lala et al., 2013).

Depending on the severity of the disease and the extent of organ involvement, different treatment strategies are used to treat GLA. Surgery and radiotherapy have been used to reduce pleural effusions and to stabilize affected regions of the skeleton (Ludwig et al., 2016; Ozeki et al., 2016). Pharmacotherapy has also been used to treat patients with GLA. The most commonly used pharmacotherapies have been zoledronic acid (osteoclast inhibitor), interferon α 2b (angiogenesis inhibitor), and rapamycin (mechanistic target of rapamycin [mTOR] inhibitor; Laverdière et al., 2000; Ozeki et al., 2007, 2016; Timke et al., 2007; Yeager et al., 2008; Adams et al., 2016; Ellati et al., 2016; Triana et al., 2017). Currently, there is no clear rationale for using specific targeted therapies in GLA.

The clinical characteristics and sporadic presentation of GLA suggest that somatic mutations could cause the disease. Here, we performed targeted high-throughput sequencing with paired blood/tissue samples and isolated lymphatic endothelial cells (LECs) to test the hypothesis that GLA is caused by somatic (postzygotic) mutations.

[1]Vascular Malformations Section, Institute of Medical and Molecular Genetics, Institute of Medical and Molecular Genetics–Instituto de Investigación PAZ, Hospital Universitario La Paz, Madrid, Spain; [2]Bioinformatics Section, Institute of Medical and Molecular Genetics, Institute of Medical and Molecular Genetics–Instituto de Investigación PAZ, Hospital Universitario La Paz, Madrid, Spain; [3]Hamon Center for Therapeutic Oncology Research, University of Texas Southwestern Medical Center, Dallas, TX; [4]Department of Pathology, Hospital Universitario La Paz, Madrid, Spain; [5]Department of Pathology, Hospital Infantil Universitario Niño Jesús, Madrid, Spain; [6]Unit of Immunology, Hospital Universitario La Paz, Madrid, Spain; [7]Structural and Functional Genomics Section, Institute of Medical and Molecular Genetics, Institute of Medical and Molecular Genetics–Instituto de Investigación PAZ, Hospital Universitario La Paz, Madrid, Spain; [8]Centro de Investigación Biomédica en Red de Enfermedades Raras, Instituto de Salud Carlos III, Madrid, Spain; [9]Department of Genetics, Instituto de Investigación Sanitaria–Fundación Jiménez Díaz Universidad Autónoma de Madrid, Madrid, Spain; [10]Clinical Genetics Section, Institute of Medical and Molecular Genetics, Institute of Medical and Molecular Genetics–Instituto de Investigación PAZ, Hospital Universitario La Paz, Madrid, Spain; [11]Vascular Anomalies Center, Plastic Surgery, Hospital Universitario La Paz, Madrid, Spain; [12]Division of Surgical Oncology, Department of Surgery, University of Texas Southwestern Medical Center, Dallas, TX.

Correspondence to Michael T. Dellinger: michael.dellinger@utsouthwestern.edu; Victor Martinez-Glez: vmartinezglez@salud.madrid.org.

Results

Nine patients with a diagnosis of GLA were clinically, radiologically, and molecularly evaluated. Clinical findings for all patients are summarized in Table 1. Radiological features commonly found in our cohort of patients are shown in Fig. 1. The cohort included five females and four males. None of the patients had a relevant family history. LMs were distributed throughout the body and showed mainly a mixed macro/microcystic phenotype. Irregular and variably sized lymphatic channels were observed by histology (Fig. 2). Five patients had bone loss in the medullary cavity, one with axial involvement and four with both axial and appendicular involvement. Patient GLA002 had both cortical and medullary bone loss. Three patients had chylous effusions. Seven patients had some degree of visceral involvement, three had associated vascular malformations, and three had skin alterations. One patient had hemothorax and another patient had a coagulopathy. None of the patients had dysmorphia or overgrowth. One patient had been previously diagnosed with complete androgen insensitivity syndrome, an X-linked disorder of sex development, and another patient had Steinert disease, the most frequent myotonic dystrophy.

Somatic mutations in the PIK3CA gene can be detected in LM samples and LM-LECs from patients with GLA

We isolated LECs from fresh tissue samples obtained from two patients with GLA (GLA054 and GLA061). GLA054-LM-LECs were isolated by FACS using a $CD31^+$, podoplanin$^+$, and $CD34^{Low}$ strategy. GLA061-LM-LECs were isolated by magnetic-activated cell sorting with antibodies against CD31 and podoplanin. The final yield of isolated LM-LECs from the total cells obtained after enzymatic digestion of the tissue was 7.4% for GLA054 and <10% for GLA061. Isolated cells showed the characteristic cobblestone morphology of endothelial cells, and the identity of the cells was confirmed by immunofluorescence staining for Lyve-1 and PROX1 (Fig. 3).

We performed high-throughput sequencing studies with GLA-LM-LECs and with tissue samples from nine patients with a clinical and radiological diagnosis of GLA. As somatic mosaicism was a theoretical possibility in this pathology, paired blood/tissue samples were studied from all patients. Our first approach was to use a hybridization-based capture custom panel of 1,370 candidate genes associated with PI3K signaling, RAS/MAPK signaling, osteoclast differentiation, and other vascular/lymphatic malformations. We refer to this panel as the gene discovery panel. We identified *PIK3CA*, a gene that encodes the p110α catalytic subunit of PI3K, as our main candidate gene. Subsequently, we designed an amplicon-based, highly targeted, ultra-deep sequencing panel to search for variants in this gene. We refer to this panel as the *PIK3CA* panel. Average read depth for the gene discovery panel was 510×. Average read depth for the *PIK3CA* panel was 13,819×. After filtering, the mean variant number per sample was 203 for the gene discovery panel and 5 for the *PIK3CA* panel.

We identified four distinct *PIK3CA* (NM_006218.2) variants (Glu542Lys, Gln546Lys, His1047Arg, and His1047Leu) in five out of nine (55.6%) patients (Table 2). The variants were detected in LM tissues and also in LECs isolated from LM tissues from two patients (GLA054-LM-LECs and GLA061-LM-LECs; Table 2). All mutations were somatic missense single nucleotide variations with a range of mosaicism between 1.1% and 23.0% in LM tissues and 28% and 33% in LM-LECs. The *PIK3CA* variants have been previously described as gain-of-function mutations in cancer (Catalogue of Somatic Mutations in Cancer database; http://cancer.sanger.ac.uk/) and *PIK3CA*-related overgrowth syndrome (PROS; Mirzaa et al., 2016; Kuentz et al., 2017). The Glu542Lys, His1047Arg, and His1047Leu variants have also been reported in isolated LMs (Luks et al., 2015). All *PIK3CA* variants were confirmed using at least one alternative method based on the alternative allele frequency from the high-throughput sequencing results. *PIK3CA* mutations were not detected in LM tissue samples from patients GLA011, GLA022, GLA038, and GLA053. *PIK3CA* mutations were not present in blood samples from any of the patients.

Excessive PI3K signaling in LECs causes lymphatic hyperplasia and dysfunction in mice

Prox1-CreER^{T2} mice have been widely used to excise *floxed* DNA sequences in LECs (Srinivasan et al., 2007; Sabine et al., 2012; James et al., 2013; Murtomaki et al., 2013). To further characterize Cre-activity in *Prox1-CreER^{T2}* mice, we bred *Prox1-CreER^{T2}* mice with *mT/mG* reporter mice and analyzed the expression pattern of GFP in multiple tissues. We found that LECs in the kidney, heart, lung, pancreas, periosteum, and skin expressed GFP (Fig. S1). These data show that *Prox1-CreER^{T2}* mice display Cre activity in LECs in multiple tissues. We also found that cardiomyocytes, hepatocytes, islets, neurons, and pancreatic ducts expressed GFP (Fig. S1). These findings are in agreement with other reports that cardiomyocytes, hepatocytes, islets, neurons, and pancreatic ducts express Prox1 (Wang et al., 2005; Risebro et al., 2009; Choi et al., 2011; Truman et al., 2012; Hong et al., 2016).

To characterize the effect of excessive PI3K signaling in LECs on the structure and function of lymphatics, we used the Cre-loxP system to express an active form of *PIK3CA* in LECs. We bred *Prox1-CreER^{T2}* mice with *LSL-Pik3ca^{H1047R}* mice (Cre-inducible mutant form of *PIK3CA*) to create *Prox1-CreER^{T2};LSL-Pik3ca^{H1047R}* mice (Fig. 4 A). *LSL-Pik3ca^{H1047R}* (control) and *Prox1-CreER^{T2};LSL-Pik3ca^{H1047R}* mice were injected with tamoxifen on postnatal days (P) 31, P33, P35, P39, and P42, and tissues were collected from mice on P70 and P98 (Fig. 4 B). Whole-mount immunofluorescence staining of ear skin revealed that the lymphatic network in *Prox1-CreER^{T2};LSL-Pik3ca^{H1047R}* mice was hyperplastic (Fig. 4, C–G). To determine whether LEC proliferation was different between *LSL-Pikc3ca^{H1047R}* and *Prox1-CreER^{T2};LSL-Pik3ca^{H1047R}* mice, we stained sections of ear skin with antibodies against Lyve-1 and Ki-67. We found that *Prox1-CreER^{T2};LSL-Pik3ca^{H1047R}* mice had significantly more Ki-67–positive LECs than *LSL-Pik3ca^{H1047R}* mice (Fig. S2). These results show that excessive PI3K signaling in LECs induces LEC proliferation.

To determine whether excessive PI3K signaling in hepatocytes and pancreatic ducts caused abnormalities, we examined H&E-stained liver and pancreas samples from *LSL-Pik3ca^{H1047R}* and *Prox1-CreER^{T2};LSL-Pik3ca^{H1047R}* mice. We did not observe any histological abnormalities in the liver and pancreas samples from *Prox1-CreER^{T2};LSL-Pik3ca^{H1047R}* mice (Fig. S3). To extend

Table 1. **Clinical features in nine patients with GLA**

Patient	Age (y)	Sex	*PIK3CA* variant	LM	Effusions	Osteolysis	Visceral involvement	Associated vascular anomalies	Skin alteration	Rapamycin treatment	Rapamycin response	Other
GLA002	17	F	c.3140A>G; p.His1047Arg	Pelvic LM (predominantly microcystic) affecting lumbosacral spine and gluteal region	–	Massive (axial and appendicular) osteolysis in iliac bones, sacro-coccygeal vertebrae and vertebral body L5, causing paraplegia of lower limbs	Pelvic organs	Atypical epidermoid hemangioma in cranial vault	Sacral patch	+	Pain reduction; improvement in ability to walk	Treatment with radiotherapy and interferon; secondary ovarian dysfunction; idiopathic intracranial hypertension; hyperthyroidism; dysmetria; distal shortening of the ulna; accessory cervical rib; scoliosis; slow growth
GLA006	23	M	c.3140A>T; p.His1047Leu	LM (predominantly macrocystic) in the arm (skin, soft tissues, and humerus), covering the right axilla, shoulder, and right hemithorax (pleura, pericardium, anterior mediastinum, thymus, diaphragm, ribs and vertebrae), and spleen	Chylothorax, hemothorax, chylopericardium	Osteolysis (axial and appendicular) of the humerus, clavicle, and ribs on the right side	Spleen	–	Upper limb	–	NA	Deceased
GLA011	20	M	None	Bilateral cervico-thoracic macrocystic LM with discrete bilateral mediastinal progression (up to aorto-pulmonary window) and around the vertebral arteries in the cranial region	–	Multiple (axial and appendicular) lytic lesions predominantly affecting dorsal and lumbar vertebrae, third left rib, pelvis, both middle thirds of humerus, bilateral supraacetabular region, and proximal portions of femurs	–	–	–	+	Pain reduction; improvement of dysphagia; breathing	Multiple cervical LM infections
GLA022	6	F	None	Right mediastinal thoracic macrocystic LM with supraclavicular and external thoracic extension; two small splenic LMs	–	–	Lung, spleen	Upper cava aneurysm	–	–	NA	Diffuse supra and infratentorial cortico-subcortical atrophy; breathing difficulties; right lung diffuse alveolar damage; squamous metaplasia and tracheobronchial ulcerations; herpes simplex virus type II ulcers in tongue; chronic duodenal peptic ulcer; thymus atrophy by compression; deceased
GLA038	15	F	None	Multiple LMs: retroperitoneal infiltrating the spine, with macrocystic component, the biggest in the left hypochondrium, right flank, and right paravesical; and microcystic, most important in soft tissues of right hemipelvis	–	Multiple (axial and appendicular) bone lesions in vertebral bodies D12, L1, L3, L4, L5, sacrum, and iliac crests	Multiple focal lesions in spleen	–	–	+	Pain reduction	Complete androgen insensitivity syndrome; hypogonadotropic hypogonadism; absence of Müllerian structures and abdominal dysplastic testicle; umbilical hernia; osteopenia
GLA051	35	F	c.1624G>A; p.Glu542Lys	Retroperitoneal and right thigh mixed (macro/microcystic) LMs	Chylous ascites	–	Kidney compression; nephrectomy	–	–	+	Pain reduction	Steinert disease; secondary lymphedema in right leg; severe chronic pain in the outer area of the right knee; epigastric hernia; surgery for polyps in the gallbladder
GLA053	4	M	None	Thoracic LM (predominantly microcystic)	Chylopericardium	Osteolysis (axial) in upper and lower part of left ribs, arches 10 to 12 missing	Left lung	–	Two large hyperchromic lesions in left hemithorax	+	Pain reduction, metabolic improvement, size reduction	Severe respiratory insufficiency; cardiac tamponade; bronchospasm; thrombopenia; failure to thrive; growth delay in size and weight, gastrostomy, and Port-a-Cath
GLA054	38	F	c.1636C>A; p.Gln546Lys	LM in left upper limb and hemithorax present since birth (predominantly microcystic)	Hemothorax	–	–	–	–	+	Pain reduction	–
GLA061	16	M	c.1624G>A; p.Glu542Lys	Cervicofacial and thoracic complex LM (mixed, with slight macrocystic predominance)	–	–	–	Cervical and cranial LVM; intracraneal VM	–	+	Pain reduction	–

F, female; LVM, lymphatic venous malformation; M, male; NA, not applicable; VM, venous malformation.

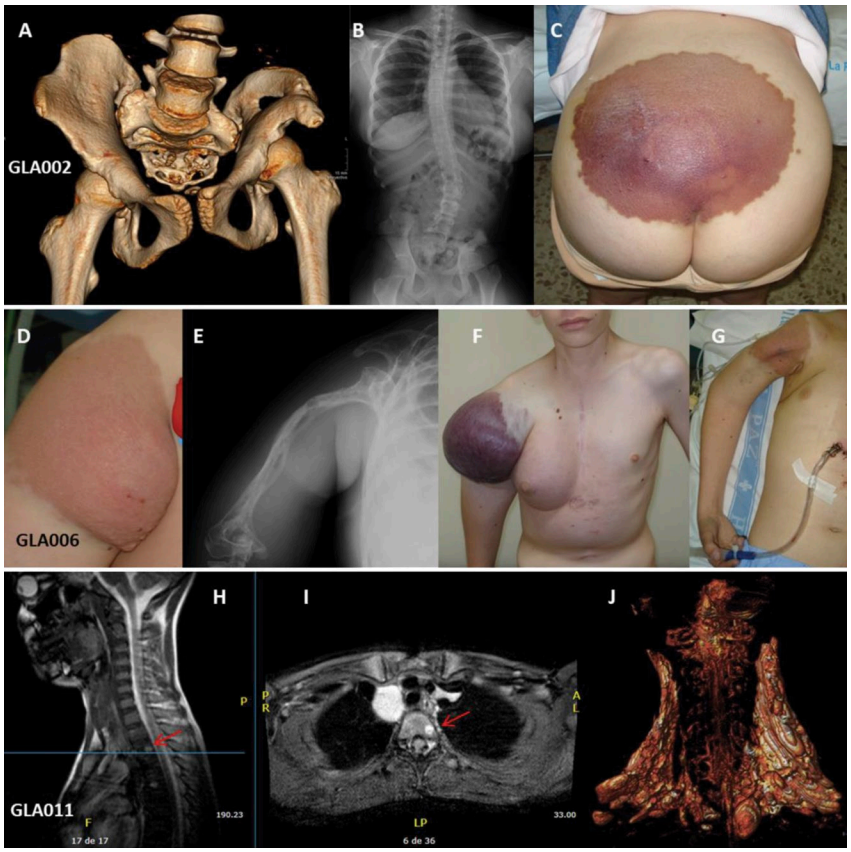

Figure 1. **Clinical manifestations in patients with GLA. (A–C)** GLA002: Pelvic lymphatic malformation with massive osteolysis (A), secondary scoliosis (B), and skin involvement (C). **(D–G)** GLA006: Cutaneous (D) and humeral involvement (E), with intralesional bleeding (F) and cardiac tamponade in the context of chylopericardium (G). **(H and I)** GLA011: Multiple lytic lesions are present in this patient. Red arrows show an osteolytic lesion adjacent to the superior vertebral plate of T2, 8 × 5 mm, without cortical or disc involvement. **(J)** A bilateral cervical LM that is more prominent on the right side than the left side.

our findings for the pancreas, we also performed an Alcian Blue stain. Alcian Blue staining is performed to identify pancreatic intraepithelial neoplasia (PanIN) lesions, which are precursors to pancreatic ductal adenocarcinoma. Importantly, we found that *Prox1-CreER^{T2};LSL-Pik3ca^{H1047R}* mice did not have PanIN lesions (Fig. S3).

Intradermally injected Evans blue dye (EBD) binds to albumin, which is absorbed and transported by lymphatic vessels. We performed bipedal EBD lymphangiography to assess lymphatic function in tamoxifen-injected mice. We found that EBD was transported from the hind paws to the iliac lymph nodes in *LSL-Pik3ca^{H1047R}* mice, but not in *Prox1-CreER^{T2};LSL-Pik3ca^{H1047R}* mice (Fig. 4, H and I). These results show that excessive PI3K signaling in LECs impairs the function of lymphatic vessels. The functional defect in *Prox1-CreER^{T2};LSL-Pik3ca^{H1047R}* mice could be due to problems with lymphatic capillaries (e.g., the capillaries are leaky or unable to take up fluid), collecting lymphatics (e.g., valve dysfunction), or both.

Excessive PI3K signaling in LECs induces the formation of lymphatics in bone

Bones in GLA patients can contain lymphatic vessels. To determine whether *Prox1-CreER^{T2};LSL-Pik3ca^{H1047R}* mice had bone involvement, we analyzed femurs from P98 mice. No lymphatic vessels were present in femurs from *LSL-Pik3ca^{H1047R}* mice (Fig. 5 A). In contrast, four out of nine *Prox1-CreER^{T2};LSL-Pik3ca^{H1047R}* mice had lymphatic vessels in their bones (Fig. 5 B). Lymphatic vessels were in the marrow cavity and cortical bone. The number of lymphatics ranged from 0 to 10 vessels per femur. Although a subset of femurs from *Prox1-CreER^{T2};LSL-Pik3ca^{H1047R}* mice had lymphatic vessels, the femurs did not display structural abnormalities and were indistinguishable from femurs from *LSL-Pik3ca^{H1047R}* mice (Fig. 5, C and D). To determine whether the severity of the bone phenotype increased with age, we attempted to collect femurs from older mice. However, we found that almost all of the tamoxifen-injected *Prox1-CreER^{T2};LSL-Pik3ca^{H1047R}* mice developed a pleural effusion and died before P98 (Fig. S4). In some *Prox1-CreER^{T2};LSL-Pik3ca^{H1047R}* mice, the effusion fluid appeared chylous, whereas in others, it appeared bloody (Fig. S4).

Rapamycin prevents lymphatic hyperplasia and dysfunction in *Prox1-CreER^{T2};LSL-Pik3ca^{H1047R}* mice

Because PI3K signaling stimulates the activation of mTOR, we set out to determine whether rapamycin could prevent lymphatic hyperplasia and dysfunction in *Prox1-CreER^{T2};LSL-Pik3ca^{H1047R}* mice. *Prox1-CreER^{T2};LSL-Pik3ca^{H1047R}* mice were injected with tamoxifen on P31, P33, P35, P39, and P42 and then treated with vehicle or rapamycin from P43 to P70 (Fig. 6 A). We found that rapamycin prevented lymphatic hyperplasia in *Prox1-CreER^{T2};LSL-Pik3ca^{H1047R}* mice (Fig. 6, B–D). To assess lymphatic function, we injected the hind paws of mice with EBD. EBD was not transported from the hind paws to the iliac lymph nodes in any of the vehicle-treated mice. In contrast, EBD was transported to the iliac lymph nodes in all of the rapamycin-treated mice (Fig. 6, E and F). These results show that rapamycin can prevent lymphatic hyperplasia and preserve lymphatic function in *Prox1-CreER^{T2};LSL-Pik3ca^{H1047R}* mice.

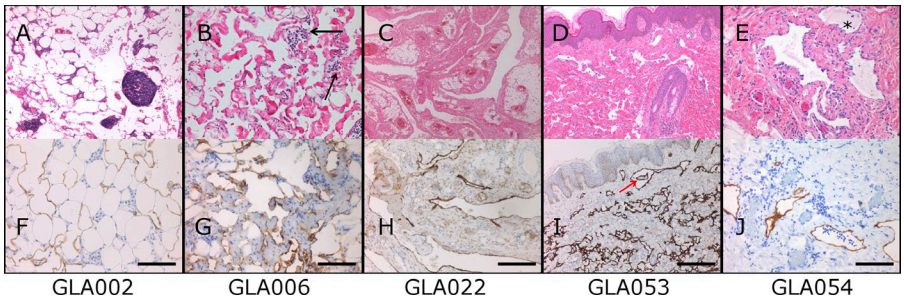

Figure 2. **Histology of GLA lesions. (A–J)** Biopsies show irregular and variably sized lymphatic channels involving skin (D and I), subcutaneous fat (A and F), and soft tissues (B and G, C and H, and E and J). The endothelial cells lining the vessels show no atypical features. The lumens are empty or filled with proteinaceous fluid, occasionally containing lymphocytes and histiocytes (GLA054, asterisk). Prominent lymphoid aggregates are noted in the stroma in some cases (GLA002). The presence of hemosiderophages indicates past hemorrhage (GLA006, black arrows). In GLA053, irregular vascular channels, more evident in the superficial dermis, show intraluminal pseudopapillae (red arrow). **(F–J)** Immunopositivity for D2-40 (brown) highlights the endothelium of lymphatic channels. Bars, 100 µm (F, G, and J); 200 µm (H and I).

Rapamycin partially restores lymphatic function in *Prox1-CreER^{T2};LSL-Pik3ca^{H1047R}* mice with established disease

Next, we set out to characterize the effect of rapamycin on the phenotype of *Prox1-CreER^{T2};LSL-Pik3ca^{H1047R}* mice with established disease. *Prox1-CreER^{T2};LSL-Pik3ca^{H1047R}* mice were injected with tamoxifen on P31, P33, P35, P39, and P42 and then treated with vehicle or rapamycin from P70 to P91 (Fig. 7 A). We found that rapamycin attenuated lymphatic hyperplasia in *Prox1-CreER^{T2};LSL-Pik3ca^{H1047R}* mice (Fig. 7, B–D). To assess lymphatic function, we injected the hind paws of mice with EBD. EBD was not transported from the hind paws to the iliac lymph nodes in any of the vehicle-treated mice. To our surprise, EBD was transported from the hind paws to the iliac lymph nodes in 9 out of 11 of the rapamycin-treated mice (Fig. 7, E and F). These results show that rapamycin can attenuate lymphatic hyperplasia and partially restore lymphatic function in *Prox1-CreER^{T2};LSL-Pik3ca^{H1047R}* mice with established disease.

Rapamycin reduces pain in patients with GLA

Seven of the nine patients with GLA were treated with rapamycin at 0.8 mg/m^2 per dose twice daily for an average time of 16 mo. All patients reported a reduction in pain, and one patient showed a subjective (not measured) decrease in the size of their LM. Additionally, three patients showed functional improvement. No improvement of chylothorax or bone regeneration was observed. With respect to side effects, ulcers were observed in the oral mucosa in all patients, and high cholesterol levels were observed in five patients. No related infections were recorded. Antibiotic prophylaxis was not given.

Discussion

In the present report, we describe the presence of somatic activating *PIK3CA* mutations in patients with GLA. The variants were detected in LM samples from five out of nine (55.6%) patients and in LECs isolated from LM samples from two patients (100%). We show that mice that express an active form of *PIK3CA* in their LECs develop hyperplastic lymphatics and lymphatics in bone. Additionally, we show that rapamycin can prevent lymphatic hyperplasia and dysfunction in our mouse model of GLA. Lastly, we show that patients with GLA respond to rapamycin. Together, this work demonstrates that GLA can be caused by somatic activating mutations in *PIK3CA* and suggests that rapamycin could be an effective treatment for GLA.

To conclude that somatic activating mutations in *PIK3CA* can cause GLA, we must be sure of the diagnosis of our cohort of patients and weigh possible differential diagnoses. The mutations in this work were detected in LM samples, and even though mutations in *PIK3CA* have already been described in isolated LMs, it is clear that the patients in our study have multifocal disease, undoubtedly differentiating them from patients with isolated LMs. It is also necessary to rule out other PROS diseases such as congenital lipomatous overgrowth, vascular malformations, epidermal nevis, and spinal/skeletal anomalies/scoliosis (CLOVES). None of the patients in our study exhibited characteristics of CLOVES such as asymmetric growth, epidermal nevi, capillary malformation, macrodactyly, sandal gap, or spinal cord involvement. Importantly, none of the patients had lipomatous overgrowth, one of the main characteristics of CLOVES.

It is more challenging to differentiate GLA from Gorham-Stout disease, which is also characterized by LMs and bone loss. Based on the current literature (Lala et al., 2013) and our own clinical experience, the patients in this cohort were diagnosed with GLA because they had different combinations of (1) multiple cystic lesions, (2) multiple, nonprogressive lytic areas in the medullary cavity, (3) concurrent axial and appendicular skeletal involvement with noncontiguous lesions, and (4) a high incidence of visceral and skin involvement, as well as other vascular malformations. This differentiates the patients in our study from patients with Gorham-Stout disease, who typically present with cortical and progressive osteolysis, adjacent soft tissue changes, and mainly axial skeletal involvement (Lala et al., 2013).

It was previously reported that GLA patients tend to have macrocystic LMs (Lala et al., 2013). However, our cohort of GLA patients had a variable combination of mixed micro/macrocystic LMs. Our observation highlights the need for additional studies focused on characterizing the phenotypic spectrum of patients with GLA. A better understanding of the phenotype of patients with GLA will facilitate the diagnosis of GLA, improve the classi-

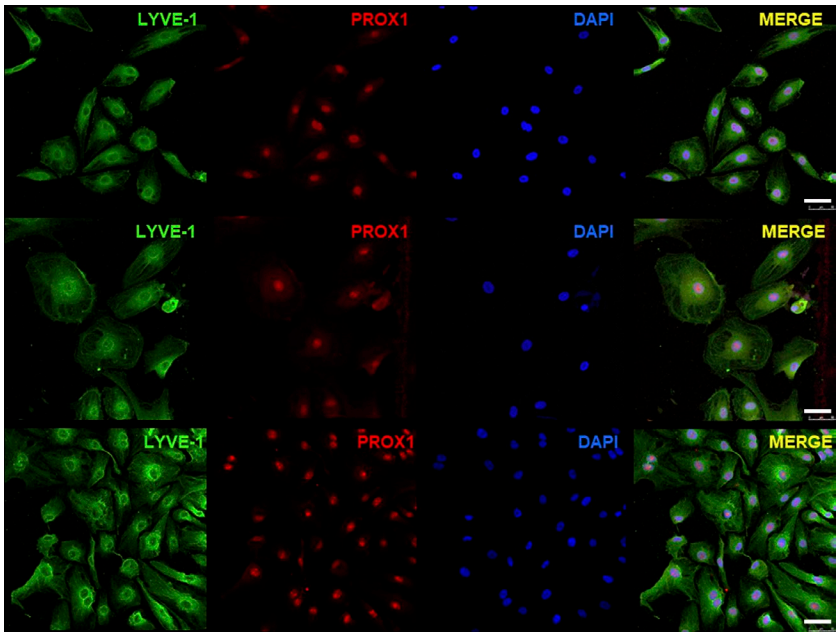

Figure 3. **Immunofluorescence staining of LECs isolated from patients with GLA.** Representative immunofluorescence images of LECs isolated from patients with GLA (GLA0054 and GLA0061), compared with commercial human dermal LECs, stained with specific markers (LYVE-1 and PROX1) and analyzed by confocal microscopy. Bars, 50 µm.

fication of lymphatic anomalies, and help define the pathophysiological aspects of the disease.

The detection of tissue-specific mutations in *PIK3CA* in our cohort of patients confirms somatic mosaicism as a pathogenic mechanism in GLA. Somatic mosaicism, defined as the presence of more than one clone of cells with different genotypes derived from a single cell, causes phenotypic variability depending on the specific tissue affected. Because of this, *PIK3CA* somatic mutations are present in patients with distinct but partially overlapping clinical features within the PROS family of developmental syndromes (Kurek et al., 2012; Lindhurst et al., 2012; Rivière et al., 2012; Keppler-Noreuil et al., 2014, 2015; Kuentz et al., 2017). This family includes different disorders in which overgrowth and/or LMs are a component feature, such as CLOVES;

Table 2. **Molecular results for *PIK3CA* in nine patients with GLA**

Patient	Age (y)	Sex	Sample	Method	Variant	Alt.var.freq% (wt;alt)
GLA002	17	F	GLA002-Bone1 (iliac crest)	HB	–	0 (186;0)
			GLA002-Bone2 (sacrum)	AB	–[a]	0.01 (38,548;5)
			GLA002-Fascia tissue	AB	–[a]	0.02 (34,032;6)
			GLA002-LM (FFPE)	AB	c.3140A>G; p.His1047Arg	23.0 (22,652;6,761)
GLA006	23	M	GLA006-LM_1	HB	–	0 (277;0)
			GLA006-LM_2 (FFPE)	AB	c.3140A>T; p.His1047Leu	18.48 (12,007;2,722)
GLA011	20	M	GLA011-LM	AB	–	–
GLA022	6	F	GLA022-LM (FFPE)	AB	–	–
GLA038	15	F	GLA038-LM	AB	–	–
GLA051	35	F	GLA051-LM	HB	c.1624G>A; p.Glu542Lys	3.5 (320;11)
			GLA051-LM	AB	c.1624G>A; p.Glu542Lys	1.1 (35,018;385)
GLA053	4	M	GLA053-LM	AB	–	–
GLA054	38	F	GLA054-LM	HB	c.1636C>A; p.Gln546Lys	3.1 (624;20)
			GLA054-LM	AB	c.1636C>A; p.Gln546Lys	3.4 (51,752;1,780)
			GLA054-LM-LECs	HB	c.1636C>A; p.Gln546Lys	27.9 (277;107)
GLA061	16	M	GLA061-LM	AB	c.1624G>A; p.Glu542Lys	1.68 (73,577;1,234)
			GLA061-LM-LECs	AB	c.1624G>A; p.Glu542Lys	33.67 (36,999;12,459)

AB, amplicon-based high-throughput sequencing; Alt.var.freq%, frequency of the alternative variant; F, female; HB, hybridization-based; M, male; wt;alt, number of reads for wild-type and alternative alleles.
[a]Next-generation sequencing reads in the background noise range of the technique and cannot be considered as positive.

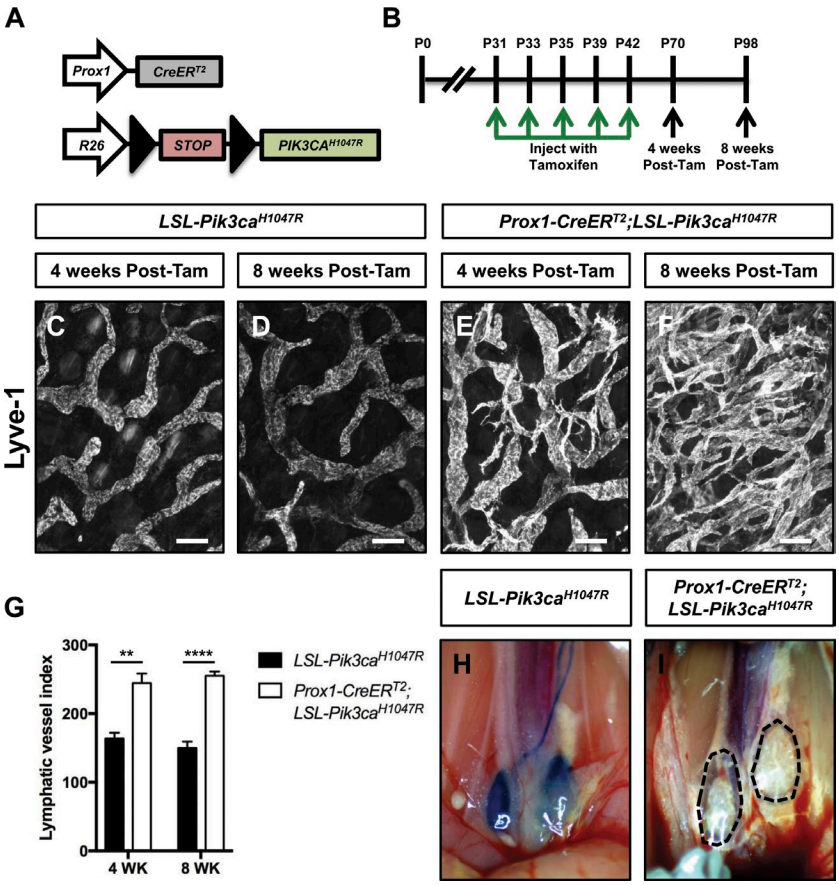

Figure 4. **Expression of *Pik3ca*^{H1047R} in LECs causes lymphatic hyperplasia and dysfunction. (A)** Schematic of the Cre-loxP system used to induce the expression of *Pik3ca*^{H1047R}. **(B)** Schematic that shows when *Pik3ca*^{H1047R} and *Prox1-CreER*^{T2}*;LSL-Pik3ca*^{H1047R} mice were injected with tamoxifen. Mice were analyzed on P70 (4 wk after the last tamoxifen injection) and P98 (8 wk after the last tamoxifen injection). Tam, tamoxifen. **(C–F)** Representative images of ear skin whole-mounts stained with an anti–Lyve-1 antibody. The lymphatic network in *Prox1-CreER*^{T2}*;LSL-Pik3ca*^{H1047R} mice becomes hyperplastic overtime. **(G)** Lymphatic vessel index values were significantly higher in P70 (244.4 ± 13.898, n = 5) and P98 (255.0 ± 6.364, n = 4) *Prox1-CreER*^{T2}*;LSL-Pik3ca*^{H1047R} mice than in P70 (163.6 ± 8.477, n = 5) and P98 (149.8 ± 9.202, n = 4) *Pik3ca*^{H1047R} mice. **(H and I)** EBD was transported to the iliac lymph nodes in P70 *Pik3ca*^{H1047R} mice (n = 5), but not in P70 *Prox1-CreER*^{T2}*;LSL-Pik3ca*^{H1047R} mice (n = 5). **, P < 0.01; ****, P < 0.0001; unpaired Student's t test. Bars, 100 µm.

Klippel-Trénaunay syndrome; and capillary malformation of the lower lip, LM of the face and neck, asymmetry, and partial/generalized overgrowth (CLAPO; Kurek et al., 2012; Rivière et al., 2012; Luks et al., 2015; Rodriguez-Laguna et al., 2018). Based on our findings, it seems appropriate to include GLA within the PROS family of diseases. This will improve the taxonomic organization of this family of disorders (Biesecker, 2018) and will allow the entire spectrum of pathologies included in PROS to benefit from advances that occur in the study and treatment of these diseases.

We did not detect *PIK3CA* mutations in four GLA patients in our study. Therefore, it is possible that GLA is a genetically heterogeneous disease. Indeed, a mutation in *NRAS* was recently found in a patient diagnosed with GLA (Manevitz-Mendelson et al., 2018). However, we did not detect pathogenic variants in *NRAS* in any of the patients in our study. It is also possible that we were unable to identify variants in *PIK3CA* or other genes because the patients were low-level mosaics or because there was a low percentage of mutant cells in the sequenced sample. A mutation in *PIK3CA* was detected in the second sample but not in the first sample from patient GLA006. This is not unusual when studying different samples from patients diagnosed with a pathology associated with somatic mosaicism. The application of improved high-throughput diagnostic technologies and bioinformatics algorithms, capable of detecting low mosaics, will likely expand the identification of *PIK3CA* mutations and facilitate the genetic counseling of affected individuals and families.

Bone loss is one of the most intriguing clinical characteristics of GLA. Our study is the first to report that bone loss is associated with mutations in *PIK3CA*. It remains to be determined why bone loss occurs in GLA and not in isolated LMs or in PROS syndromes with more pleiotropic clinical features.

Lymphatic vessels are not present in normal bones, but they are present in bones in patients with GLA (Edwards et al., 2008; Lala et al., 2013). We found that *Prox1-CreER*^{T2}*;LSL-Pik3ca*^{H1047R} mice developed lymphatic vessels in their bones. Although *Prox1-CreER*^{T2}*;LSL-Pik3ca*^{H1047R} mice had lymphatic vessels in their bones, they did not lose bone. This is likely because the mice died before they had significant bone involvement. In the future, LECs from *Prox1-CreER*^{T2}*;LSL-Pik3ca*^{H1047R} mice could be isolated and injected into the tibias of wild-type mice. This approach was recently used to show that LECs induce osteoclast-mediated bone resorption in mice (Wang et al., 2017) and could reveal the effect of GLA-LECs on bone structure.

Rapamycin is a US Food and Drug Administration–approved mTOR inhibitor. We show that rapamycin suppresses lymphatic hyperplasia and dysfunction in *Prox1-CreER*^{T2}*;LSL-Pik3ca*^{H1047R} mice. We also report that rapamycin reduces pain in patients with GLA. Although this work is not a controlled clinical trial, it adds to the growing number of reports that GLA patients respond to rapamycin (Hammill et al., 2011; Adams et al., 2016; Triana et al., 2017). Interestingly, we found that patients in whom we did not detect a mutation in *PIK3CA* responded to rapamycin. This could be due to other types of alterations in *PIK3CA* that we were not able to detect or to alterations in other components in the PI3K/AKT pathway that activate mTOR. Future studies will help distinguish between these two possibilities.

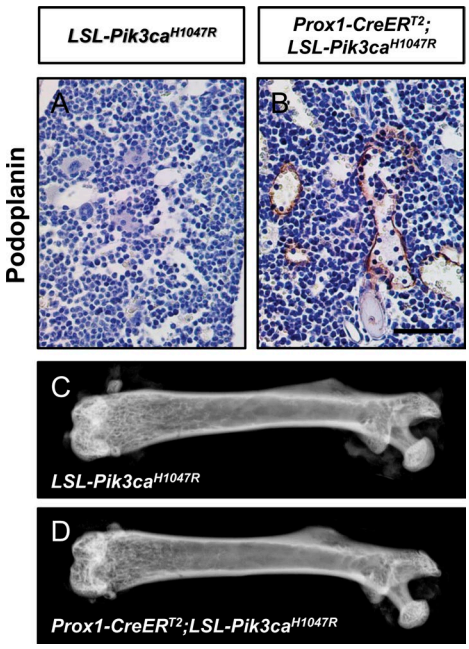

Figure 5. ***Prox1-CreER^{T2};LSL-Pik3ca^{H1047R}* mice have lymphatics in their bones. (A and B)** Representative images of femurs stained with an anti-podoplanin antibody. Femurs from *Prox1CreER^{T2};LSL-Pik3ca^{H1047R}* mice (four out of nine mice), but not from *LSL-Pik3ca^{H1047R}* mice, had lymphatics. **(C and D)** Representative x-ray images of femurs from *LSL-Pik3ca^{H1047R}* and *Prox1-CreER^{T2};LSL-Pik3ca^{H1047R}* mice. Femurs from *LSL-Pik3ca^{H1047R}* and *Prox1-CreER^{T2};LSL-Pik3ca^{H1047R}* mice appear similar to one another. Bar, 50 µm.

A significant part of the management of GLA could become nonsurgical in the near future. Less aggressive treatments such as interventional radiology procedures and pharmacological therapies are improving the mortality rates and the quality of life of patients. Rapamycin has become a new therapeutic option for patients with GLAs that are refractory to standard care. However, indications for rapamycin treatment in patients with GLA are not standardized. The most common indication for its use is the presence of severe chronic pain, but it is also used for progressive osteolysis, respiratory failure, and different types of lymphatic leaks. Importantly, it is a safe treatment showing minimal side effects when administered in neonates and young infants for long periods of time (Nadal et al., 2016). Unfortunately, the specific phenotypes that respond to treatment, the optimum dose of rapamycin, and the duration of treatment remain unclear. Customized controlled trials will help answer these questions and lead to the development of specific treatment protocols for GLA.

Materials and methods

Patients and samples

Participants were seen at the Vascular Anomalies Center and the Institute of Medical and Molecular Genetics and had a clinical diagnosis of GLA. All studies in this project were approved by the Ethics Committee of the Hospital Universitario La Paz (reference PI-1404). Informed consent was obtained from all patients/parents. GLA was diagnosed based on the presence of a combination of diffuse or multicentric proliferation of dilated lymphatic vessels, progressive osteolysis, and skin/visceral compromise (Lala et al., 2013; Trenor and Chaudry, 2014). We retrospectively reviewed the clinical characteristics of nine patients diagnosed with GLA between December 2012 and September 2017. Blood and tissue samples were collected from patients with GLA during surgical procedures scheduled as part of their routine treatment. LECs were also isolated from LM tissues from two patients (GLA054 and GLA061). When available, archived formalin-fixed, paraffin-embedded (FFPE) tissue samples were retrospectively collected from La Paz Hospital Biobank. All samples studied for each patient are described in Table 1. DNA extraction was performed by standard procedures. We first performed high-throughput sequencing studies with a large custom panel for gene discovery. After we identified the candidate gene, we performed targeted, ultra-deep sequencing, and the candidate variants were later validated by Sanger sequencing, pyrosequencing, and/or droplet digital PCR (ddPCR) depending on the degree of mosaicism detected.

High-throughput sequencing

High-throughput sequencing studies were performed using two different platforms. In the first platform, we used a hybridization-based capture approach for gene discovery, including 1,370 genes associated with PI3K signaling, RAS/MAPK signaling, osteoclast differentiation, and other related vascular malformations. The custom panel was designed with NimbleDesign (https://design.nimblegen.com; Roche NimbleGen): HG19 NCBI Build 37.1/GRCh37, targeting >98% of all exons (RefSeq) for these genes. For each sample, paired-end libraries (2 × 150 bp reads) were created according to the standard deep sequencing protocols KAPA HTP Library Preparation Kit for Illumina platforms, SeqCap EZ Library SR (Roche NimbleGen) and NEXTflex-96 Pre Capture Combo Kit (Bioo Scientific Corp.) for indexing. The captured DNA samples were sequenced on a NextSeq 500 instrument (Illumina) using a HIGH v2 300 cycles cartridge, according to the standard operating protocol.

In the second platform, we used an amplicon-based method for highly targeted, ultra-deep sequencing, including *PIK3CA* and another 19 related genes. For this panel, probes were designed with the DesignStudio Sequenced Assay tool (Illumina), using an amplicon length of 175 bp and a total number of 715 amplicons. The dual-pool design was selected, and amplicon-based library preparation was performed using the TruSeq Custom Amplicon Low Input Kit according to the manufacturer's protocol (Illumina). The protocol starts from 10 ng of genomic DNA or FFPE DNA samples. To optimize the variant detection and minimize false-positive reads (artifacts), a second pool of oligos with the same samples were synthesized and sequenced in parallel, which is especially helpful in FFPE samples. The captured DNA samples were sequenced on a NextSeq 500 instrument using a Mid Output kit v2 300 cycles cartridge, according to the standard operating protocol.

Bioinformatics analysis

Two different bioinformatic analyses were applied, depending on the high-throughput sequencing platform used. For the hybridization-based capture approach, data generated by the NextSeq 500 Desktop Sequencer was analyzed using an in-house bioin-

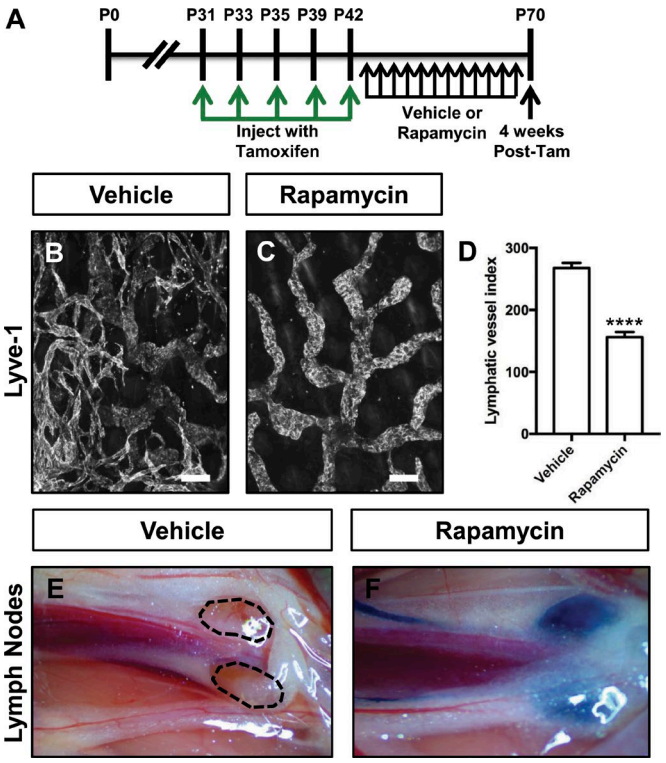

Figure 6. **Rapamycin prevents lymphatic hyperplasia and dysfunction in *Prox1-CreER^{T2};LSL-Pik3ca^{H1047R}* mice. (A)** Schematic that shows when mice were injected with tamoxifen. *Prox1-CreER^{T2};LSL-Pik3ca^{H1047R}* mice were treated with vehicle or rapamycin (100 µg; 5×/wk) from P43 to P70. Tam, tamoxifen. **(B and C)** Representative images of ear skin whole-mounts stained with an anti–Lyve-1 antibody. The lymphatic network was hyperplastic in vehicle-treated mice but not in rapamycin-treated mice. **(D)** Lymphatic vessel index values were significantly higher in vehicle-injected mice (267.7 ± 8.293, n = 3) than in rapamycin-injected mice (156 ± 8.269, n = 7). **(E and F)** EBD was transported to the iliac lymph nodes in rapamycin-treated mice (n = 7), but not in vehicle-treated mice (n = 4). ****, P < 0.0001, unpaired Student's t test). Bars, 100 µm.

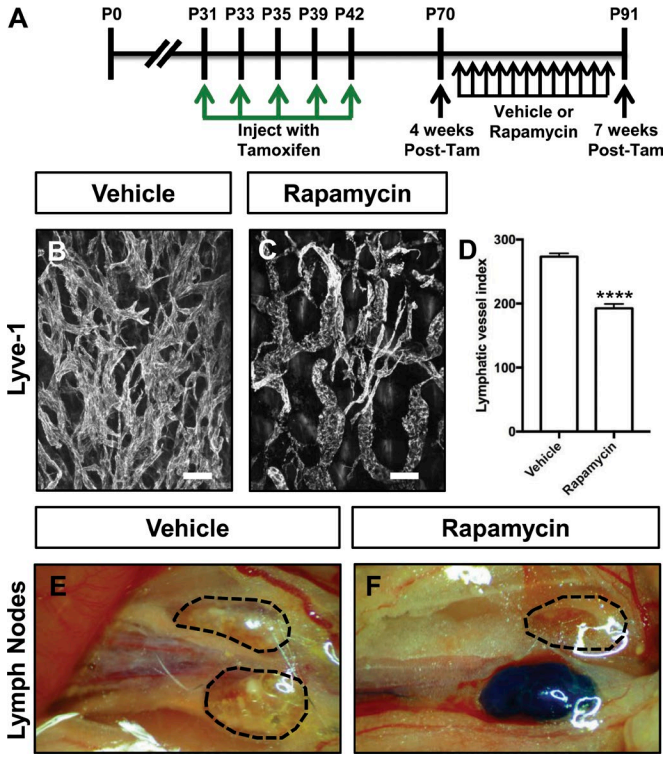

Figure 7. **Rapamycin attenuates lymphatic hyperplasia and restores lymphatic function in *Prox1-CreER^{T2};LSL-Pik3ca^{H1047R}* mice. (A)** Schematic that shows when mice were injected with tamoxifen. *Prox1-CreER^{T2};LSL-Pik3ca^{H1047R}* mice were treated with vehicle or rapamycin (100 µg; 5×/wk) from P70 to P91. Tam, tamoxifen. **(B and C)** Representative images of ear skin whole-mounts stained with an anti–Lyve-1 antibody. **(D)** Lymphatic vessel index values were significantly higher in vehicle-injected mice (273 ± 5.404, n = 6) than in rapamycin-injected mice (192.5 ± 6.876, n = 7). **(E and F)** EBD was transported to the iliac lymph nodes in most rapamycin-treated mice (9 out of 11 mice). In contrast, EBD was not transported to the iliac lymph nodes in vehicle-treated mice (n = 9). ****, P < 0.0001; unpaired Student's t test). Bars, 100 µm.

formatics pipeline for somatic mosaicism detection. In brief, BCL files containing base calls were converted into paired FASTQ files using bcl2fastq-v2.15.0.4 software from Illumina (https://github.com/brwnj/bcl2fastq) and preprocessing using Trimmomatic for trimming and cropping FASTQ data as well as removing adapters. Subsequently, balanced reads were mapped to hg19/GRCh37 human genome by using Bowtie2 aligner, and PCR duplicate reads were removed using Picard MarkDuplicates. A subsequent local realignment and recalibration of reads was done to correct misalignments due to the presence of INDELs by using GATK RealignerTargetCreator and IndelRealigner, and BaseRecalibrator methods, respectively. Mosaic detection included the extraction of the bp information for each genomic position from the BAM files using samtools mpileup v1.3, facilitating the subsequent SNP/INDEL calling. Variant calling was performed using bcftools v1.3. The strategy of the analysis was to keep all multiallelic sites in the VCF file for later consideration. Some attributes were defined to filter out likely sequencing artifacts or variants with high frequency in samples sequenced in the same run, and others to keep mosaic variants to analyze further on. Subsequently, a germline versus somatic variant comparison was undertaken by analyzing the tissue and the blood VCF files from the same patient/sample. The final files encoded global information about alignments. Manual filtering was applied to determine the candidate pathogenic variants. The resulting VCF files were manually visualized with the Integrative Genomics Viewer software to verify mutations and correct annotation. For the amplicon-based method, a different analysis strategy was followed. BCL files resulting from the NextSeq 500 were converted into paired FASTQ files using bcl2fastq-v2.15.0.4 software from Illumina. After that, three bioinformatic apps from Illumina (Amplicon Ds tool, Variant Calling Assessment tool, and TruSeq Amplicon tool) were used to obtained VCF files. Alignment was performed using the banded Smith-Waterman algorithm in the targeted regions, and the variant calling used the Illumina-developed Somatic Variant Caller and the Ensembl database for the annotation of the variants.

Validation of high-throughput deep sequencing variants

Variants present in >15% of the reads in the deep sequencing data were confirmed by Sanger sequencing using the 96-capillary ABI 3730xl ADN analyzer (Applied Biosystems). Mosaics variants in

the 5% and 15% read fraction range were confirmed by pyrosequencing. Primers were designed using PyroMark software, and QIAGEN reagents and the Pyromark Q96 MD instrument (QIAGEN) were used according to the manufacturer's protocol. Variants found in <5% of reads were confirmed by ddPCR. The QX200 Droplet Digital PCR System (Bio-Rad) was used to generate DNA-oil droplets and posterior variant quantification using a two-color fluorescence detector, according to the manufacturer's protocol. In addition to including a control sample in each experiment, six assays with well-defined and validated somatic mosaic variants were used as controls to previously validate the technique.

Isolation and characterization of LM-LECs in patients with GLA

Fresh tissues obtained from surgical procedures were immersed in EGM-2MV BulletKit Medium after collection and transported immediately to the laboratory. Tissues were dissected into 1-mm^3 pieces and incubated with PBS containing 0.1% collagenase for 1–2 h at 37°C. The digested cell suspensions were gently squeezed through a 70-µm nylon cell strainer, centrifuged at 300 *g* for 10 min, and resuspended in EGM-2MV BulletKit Medium. To reduce fibroblast and other cell type contamination, a Percoll gradient centrifugation was performed. Percoll gradients ranged from 45% to 15% Percoll in 5% steps of 5.0 ml each except 9.0 ml in the 15% step. The endothelial cell–containing section was recovered between the 30% and 35% gradient (adaptation from Gu et al., 2006). Cells were seeded in a Petri dish for 30 min to remove fast-adhering cells for further reduce fibroblast contamination. The unbound cells were removed into a sterile Falcon tube, pelleted, and resuspended in EGM-2MV supplemented with vascular endothelial growth factor–C before being seeded in fibronectin-coated plastic. For the isolation of the GLA054-LM-LECs, a FACS strategy was applied, as described before (Lokmic et al., 2015), using anti-human podoplanin (Sigma-Aldrich)–Alexa Fluor 488 (1:200; Cell Signaling), Brilliant Violet 421 anti-human CD34 antibody (1:200; BioLegend), PE mouse anti-human CD31 (1:50; Becton Dickinson), and 7AAD PerCP (1:20; BioLegend). For the isolation of GLA061-LM-LECs, a CD31-positive, podoplanin-positive selection strategy was employed using antibody-coated magnetic beads (Dynabeads; Invitrogen, Life Technologies) to separate LECs from other cell types (Osborn et al., 2015). The purity and phenotype of the isolated LECs were confirmed by immunofluorescence staining with antibodies against PROX-1 (Abcam) and LYVE-1 (ATGen).

Rapamycin treatment in patients

Seven of the nine patients with GLA were treated with rapamycin at 0.8 mg/m^2 per dose twice daily for an average time of 16 mo. Blood levels were maintained between 12 and 20 ng/ml. To verify the response to treatment, we evaluated pain reduction, a decrease in size (subjective), functional improvement, bone regeneration, and/or improvement of chylothorax.

Mice and genotyping

The animal experiments described in this manuscript were performed in accordance with an animal protocol approved by the Institutional Animal Care and Use Committee of University of Texas Southwestern Medical Center. Mice were maintained in ventilated microsolator cages and were fed a standard diet ad libitum. Mice were provided nestlets and igloos as enrichment items. *Prox1-CreER^{T2}* mice (Srinivasan et al., 2007) were genotyped with the following primers: 5′-GTGGAAAGGAGCGTACACTGA-3′; 5′-CACACACACACACGCTTGC-3′; and 5′-GCCAGAGGCCACTTGTGTAG-3′. The wild-type allele was 370 bp, and the Cre allele was 267 bp. *LSL-Pik3ca^{H1047R}* mice (Adams et al., 2011) were genotyped with the following primers: 5′-GCGAAGAGTTTGTCCTCAACC-3′; 5′-AAAGTCGCTCTGAGTTGTTAT-3′; and 5′-GGAGCGGGAGAAATGGATATG-3′. The wild-type allele was ∼650 bp, and the mutant allele was 340 bp. *mT/mG* mice (Muzumdar et al., 2007) were genotyped with the following primers: 5′-CTCTGCTGCCTCCTGGCTTCT-3′; 5′-CGAGGCGGATCACAAGCAATA-3′; and 5′-TCAATGGGCGGGGGTCGTT-3′. The wild-type allele was 330 bp, and the mutant allele was 250 bp. All mice were maintained on a mixed genetic background (129 and FVB). Littermates were used as controls in all of our animal experiments.

Preparation of tamoxifen and rapamycin

Tamoxifen (20 mg; T5648; Sigma-Aldrich) was dissolved in a mixture of ethanol (100 µl; E7023; Sigma-Aldrich) and sunflower oil (900 µl; W530285; Sigma-Aldrich). Mice received 100 µl of tamoxifen via an intraperitoneal injection on P31, P33, P35, P39, and P42. Rapamycin (BML-A275-0025; Enzo) was dissolved in ethanol to make a stock solution (50 mg/ml). The stock solution was then diluted to 1 mg/ml in a saline solution that contained polyethylene glycol (5% wt/vol; 88440; Sigma-Aldrich) and Tween 80 (5% wt/vol; P4780; Sigma-Aldrich). Mice received 100 µg of rapamycin (∼5 mg/kg) five times a wk via an intraperitoneal injection.

Whole-mount immunofluorescence staining

Ear skin samples were fixed overnight at 4° C with 1% paraformaldehyde, washed with PBS (6 × 15 min), and then blocked overnight with PBS + 0.3% TX-100 + 20% Aquablock. Next, samples were incubated overnight with a goat anti–Lyve-1 antibody (1:1,000; AF2125; R&D Systems). Following the overnight incubation, samples were washed with PBS + 0.3% TX-100 (3 × 40 min), incubated overnight with an FITC-conjugated anti-goat antibody (1:500), and then washed with PBS + 0.3% TX-100 (3 × 40 min). Samples were mounted with ProLong Gold plus DAPI (P36935; Invitrogen).

Quantification of lymphatic vessel index

To quantify lymphatic vessels, we took representative pictures of the lymphatic network at the periphery of the ear. The pictures were analyzed with ImageJ. A grid (19,000 cm^2) was placed over the pictures, and the number of times the gridlines intersected on a lymphatic vessel was determined.

Assessment of LEC proliferation

Ear sections were stained with antibodies against Lyve-1 (1:250; AF2125; R&D Systems) and Ki-67 (1:400; 12202S; Cell Signaling). Four pictures were taken of each sample at ×20 magnification. The number of Ki-67–positive and Ki-67–negative LECs in each image was manually counted. The percentage of Ki-67–positive

LECs was determined by dividing the number of Ki-67–positive LECs by the total number of LECs.

Immunohistochemistry of bone sections

Bones were fixed in 4% paraformaldehyde overnight and then decalcified in 10% EDTA (pH, 7.4) for 2 wk. Bones were embedded in paraffin and sectioned at 5 µm. Slides were deparaffinized in xylene and rehydrated through a descending ethanol series. Endogenous peroxidase activity was blocked with a hydrogen peroxide/methanol solution, and nonspecific binding was blocked with Tris-buffered saline and Tween 20 + 20% Aquablock (PP82-T3082; East Coast Biologics). Slides were incubated overnight with a hamster anti-podoplanin antibody (1:1,000; ab11936; Abcam). The following day, slides were washed with Tris-buffered saline and Tween 20 and incubated with an HRP-conjugated secondary antibody. Antibody binding was detected with 3-3′-diaminobenzidine (SK-4105; Vector). Slides were then counterstained with hematoxylin, dehydrated through an ascending ethanol series, and cleared in xylene. Coverslips were mounted with Cytoseal.

Bipedal EBD lymphangiography

EBD (E2129; Sigma-Aldrich) was dissolved in sterile PBS to create a 1% wt/vol working solution. Mice were anesthetized with an intraperitoneal injection of avertin. Approximately 30 µl of EBD was injected intradermally into each hind paw. 3 min later, the iliac lymph nodes were examined under a dissecting microscope.

Statistical analysis of animal experiments

Data were analyzed using GraphPad Prism statistical analysis software (version 7.0). All results are expressed as means ± SEM. Unpaired Student's *t* tests were performed to test means for significance. Data were considered significant at $P < 0.05$.

Online supplemental material

Fig. S1 shows that Cre-mediated recombination occurs in LECs and other cell types in *Prox1-CreER^{T2}* mice. Fig. S2 shows that LEC proliferation is increased in *Prox1-CreER^{T2};LSL-Pik3ca^{H1047R}* mice. Fig. S3 shows that liver and pancreas samples from *Prox1-CreER^{T2};LSL-Pik3ca^{H1047R}* mice appear normal. Fig. S4 shows a survival curve for *Prox1-CreER^{T2};LSL-Pik3ca^{H1047R}* mice.

Acknowledgments

We thank all patients and their families for their participation in this study.

This work was funded by The Lymphatic Malformation Institute (Ref. PI-1404).

The authors declare no competing financial interests.

Author contributions: P. Lapunzina, J.C. Lopez-Gutierrez, and V. Martinez-Glez designed and supervised the study. L. Rodriguez-Laguna, M.T. Dellinger, and V. Martinez-Glez wrote the manuscript. C. Ayuso critically revised the study and the manuscript for intellectual content. N. Agra, G. Oliva-Molina, and G. Herranz performed in vitro cellular studies. J.M. Torres Canizalez and R. Rodríguez Pena designed and supervised flow cytometry experiments. L. Rodriguez-Laguna and N. Agra participated in the draft of the manuscript. P. Lapunzina, J.C. Lopez-Gutierrez, and V. Martinez-Glez evaluated patients and collaborated in the clinical characterization of the patients. M. Beato and I. Colmenero performed histopathological studies. E. Vallespín supervised and R. Martín-Arenas performed the high-throughput sequencing experiments. A. Bustamante supervised and C. Villaverde, G. Gordo, and L. Rodriguez-Laguna performed ddPCR experiments. K. Ibañez, A. del Pozo, and L. Rodriguez-Laguna performed the bioinformatic analysis, and L. Rodriguez-Laguna, G. Gordo, K. Ibañez, and A. del Pozo developed the in-house bioinformatic pipelines for low-mosaics detection. G. Gordo and L. Rodriguez-Laguna performed molecular experiments and analysis other than high-throughput sequencing (Sanger sequencing, pyrosequencing, etc.). N. Khurana, D. Hominick, and M.T. Dellinger performed animal studies. All authors have approved the manuscript for submission.

Submitted: 17 July 2018
Revised: 10 October 2018
Accepted: 29 November 2018

References

Adams, D.M., C.C. Trenor III, A.M. Hammill, A.A. Vinks, M.N. Patel, G. Chaudry, M.S. Wentzel, P.S. Mobberley-Schuman, L.M. Campbell, C. Brookbank, et al. 2016. Efficacy and Safety of Sirolimus in the Treatment of Complicated Vascular Anomalies. *Pediatrics*. 137:e20153257. https://doi.org/10.1542/peds.2015-3257

Adams, J.R., K. Xu, J.C. Liu, N.M. Agamez, A.J. Loch, R.G. Wong, W. Wang, K.L. Wright, T.F. Lane, E. Zacksenhaus, and S.E. Egan. 2011. Cooperation between Pik3ca and p53 mutations in mouse mammary tumor formation. *Cancer Res.* 71:2706–2717. https://doi.org/10.1158/0008-5472.CAN-10-0738

Biesecker, L.G. 2018. Mosaic disorders and the taxonomy of human disease. *Genet. Med.* 20:800–801. https://doi.org/10.1038/gim.2017.213

Choi, I., H.K. Chung, S. Ramu, H.N. Lee, K.E. Kim, S. Lee, J. Yoo, D. Choi, Y.S. Lee, B. Aguilar, and Y.K. Hong. 2011. Visualization of lymphatic vessels by Prox1-promoter directed GFP reporter in a bacterial artificial chromosome-based transgenic mouse. *Blood*. 117:362–365. https://doi.org/10.1182/blood-2010-07-298562

Edwards, J.R., K. Williams, L.G. Kindblom, J.M. Meis-Kindblom, P.C. Hogendoorn, D. Hughes, R.G. Forsyth, D. Jackson, and N.A. Athanasou. 2008. Lymphatics and bone. *Hum. Pathol.* 39:49–55. https://doi.org/10.1016/j.humpath.2007.04.022

Ellati, R., A. Attili, H. Haddad, M. Al-Hussaini, and A. Shehadeh. 2016. Novel approach of treating Gorham-Stout disease in the humerus--Case report and review of literature. *Eur. Rev. Med. Pharmacol. Sci.* 20:426–432.

Gu, B., J.S. Alexander, Y. Gu, Y. Zhang, D.F. Lewis, and Y. Wang. 2006. Expression of lymphatic vascular endothelial hyaluronan receptor-1 (LYVE-1) in the human placenta. *Lymphat. Res. Biol.* 4:11–17. https://doi.org/10.1089/lrb.2006.4.11

Hammill, A.M., M. Wentzel, A. Gupta, S. Nelson, A. Lucky, R. Elluru, R. Dasgupta, R.G. Azizkhan, and D.M. Adams. 2011. Sirolimus for the treatment of complicated vascular anomalies in children. *Pediatr. Blood Cancer.* 57:1018–1024. https://doi.org/10.1002/pbc.23124

Hong, M., E. Jung, S. Yang, W. Jung, Y.J. Seong, E. Park, A. Bramos, K.E. Kim, S. Lee, G. Daghlian, et al. 2016. Efficient Assessment of Developmental, Surgical and Pathological Lymphangiogenesis Using a Lymphatic Reporter Mouse and Its Embryonic Stem Cells. *PLoS One.* 11:e0157126. https://doi.org/10.1371/journal.pone.0157126

James, J.M., A. Nalbandian, and Y.S. Mukouyama. 2013. TGFβ signaling is required for sprouting lymphangiogenesis during lymphatic network development in the skin. *Development.* 140:3903–3914. https://doi.org/10.1242/dev.095026

Keppler-Noreuil, K.M., J.C. Sapp, M.J. Lindhurst, V.E. Parker, C. Blumhorst, T. Darling, L.L. Tosi, S.M. Huson, R.W. Whitehouse, E. Jakkula, et al. 2014.

Clinical delineation and natural history of the PIK3CA-related overgrowth spectrum. *Am. J. Med. Genet. A.* 164A:1713–1733. https://doi.org/10.1002/ajmg.a.36552

Keppler-Noreuil, K.M., J.J. Rios, V.E. Parker, R.K. Semple, M.J. Lindhurst, J.C. Sapp, A. Alomari, M. Ezaki, W. Dobyns, and L.G. Biesecker. 2015. PIK3CA-related overgrowth spectrum (PROS): diagnostic and testing eligibility criteria, differential diagnosis, and evaluation. *Am. J. Med. Genet. A.* 167A:287–295. https://doi.org/10.1002/ajmg.a.36836

Kuentz, P., J. St-Onge, Y. Duffourd, J.B. Courcet, V. Carmignac, T. Jouan, A. Sorlin, C. Abasq-Thomas, J. Albuisson, J. Amiel, et al. 2017. Molecular diagnosis of PIK3CA-related overgrowth spectrum (PROS) in 162 patients and recommendations for genetic testing. *Genet. Med.* 19:989–997. https://doi.org/10.1038/gim.2016.220

Kurek, K.C., V.L. Luks, U.M. Ayturk, A.I. Alomari, S.J. Fishman, S.A. Spencer, J.B. Mulliken, M.E. Bowen, G.L. Yamamoto, H.P. Kozakewich, and M.L. Warman. 2012. Somatic mosaic activating mutations in PIK3CA cause CLOVES syndrome. *Am. J. Hum. Genet.* 90:1108–1115. https://doi.org/10.1016/j.ajhg.2012.05.006

Lala, S., J.B. Mulliken, A.I. Alomari, S.J. Fishman, H.P. Kozakewich, and G. Chaudry. 2013. Gorham-Stout disease and generalized lymphatic anomaly--clinical, radiologic, and histologic differentiation. *Skeletal Radiol.* 42:917–924. https://doi.org/10.1007/s00256-012-1565-4

Laverdière, C., M. David, J. Dubois, P. Russo, L. Hershon, and J.G. Lapierre. 2000. Improvement of disseminated lymphangiomatosis with recombinant interferon therapy. *Pediatr. Pulmonol.* 29:321–324. https://doi.org/10.1002/(SICI)1099-0496(200004)29:4%3C321::AID-PPUL13%3E3.0.CO;2-C

Lindhurst, M.J., V.E. Parker, F. Payne, J.C. Sapp, S. Rudge, J. Harris, A.M. Witkowski, Q. Zhang, M.P. Groeneveld, C.E. Scott, et al. 2012. Mosaic overgrowth with fibroadipose hyperplasia is caused by somatic activating mutations in PIK3CA. *Nat. Genet.* 44:928–933. https://doi.org/10.1038/ng.2332

Lokmic, Z., E.S. Ng, M. Burton, E.G. Stanley, A.J. Penington, and A.G. Elefanty. 2015. Isolation of human lymphatic endothelial cells by multi-parameter fluorescence-activated cell sorting. *J. Vis. Exp.* 1:e52691.

Ludwig, K.F., T. Slone, K.B. Cederberg, A.T. Silva, and M. Dellinger. 2016. A new case and review of chylothorax in generalized lymphatic anomaly and Gorham-Stout disease. *Lymphology.* 49:73–84.

Luks, V.L., N. Kamitaki, M.P. Vivero, W. Uller, R. Rab, J.V. Bovée, K.L. Rialon, C.J. Guevara, A.I. Alomari, A.K. Greene, et al. 2015. Lymphatic and other vascular malformative/overgrowth disorders are caused by somatic mutations in PIK3CA. *J. Pediatr.* 166:1048–54.e1: 5. https://doi.org/10.1016/j.jpeds.2014.12.069

Manevitz-Mendelson, E., G.S. Leichner, O. Barel, I. Davidi-Avrahami, L. Ziv-Strasser, E. Eyal, I. Pessach, U. Rimon, A. Barzilai, A. Hirshberg, et al. 2018. Somatic NRAS mutation in patient with generalized lymphatic anomaly. *Angiogenesis.* 21:287–298. https://doi.org/10.1007/s10456-018-9595-8

Mirzaa, G., A.E. Timms, V. Conti, E.A. Boyle, K.M. Girisha, B. Martin, M. Kircher, C. Olds, J. Juusola, S. Collins, et al. 2016. *PIK3CA*-associated developmental disorders exhibit distinct classes of mutations with variable expression and tissue distribution. *JCI Insight.* 1:e87623. https://doi.org/10.1172/jci.insight.87623

Murtomaki, A., M.K. Uh, Y.K. Choi, C. Kitajewski, V. Borisenko, J. Kitajewski, and C.J. Shawber. 2013. Notch1 functions as a negative regulator of lymphatic endothelial cell differentiation in the venous endothelium. *Development.* 140:2365–2376. https://doi.org/10.1242/dev.083865

Muzumdar, M.D., B. Tasic, K. Miyamichi, L. Li, and L. Luo. 2007. A global double-fluorescent Cre reporter mouse. *Genesis.* 45:593–605. https://doi.org/10.1002/dvg.20335

Nadal, M., B. Giraudeau, E. Tavernier, A.P. Jonville-Bera, G. Lorette, and A. Maruani. 2016. Efficacy and Safety of Mammalian Target of Rapamycin Inhibitors in Vascular Anomalies: A Systematic Review. *Acta Derm. Venereol.* 96:448–452. https://doi.org/10.2340/00015555-2300

Osborn, A.J., P. Dickie, D.E. Neilson, K. Glaser, K.A. Lynch, A. Gupta, and B.H. Dickie. 2015. Activating PIK3CA alleles and lymphangiogenic phenotype of lymphatic endothelial cells isolated from lymphatic malformations. *Hum. Mol. Genet.* 24:926–938. https://doi.org/10.1093/hmg/ddu505

Ozeki, M., M. Funato, K. Kanda, M. Ito, T. Teramoto, H. Kaneko, T. Fukao, and N. Kondo. 2007. Clinical improvement of diffuse lymphangiomatosis with pegylated interferon alfa-2b therapy: case report and review of the literature. *Pediatr. Hematol. Oncol.* 24:513–524. https://doi.org/10.1080/08880010701533603

Ozeki, M., A. Fujino, K. Matsuoka, S. Nosaka, T. Kuroda, and T. Fukao. 2016. Clinical Features and Prognosis of Generalized Lymphatic Anomaly, Kaposiform Lymphangiomatosis, and Gorham-Stout Disease. *Pediatr. Blood Cancer.* 63:832–838. https://doi.org/10.1002/pbc.25914

Risebro, C.A., R.G. Searles, A.A. Melville, E. Ehler, N. Jina, S. Shah, J. Pallas, M. Hubank, M. Dillard, N.L. Harvey, et al. 2009. Prox1 maintains muscle structure and growth in the developing heart. *Development.* 136:495–505. https://doi.org/10.1242/dev.030007

Rivière, J.B., G.M. Mirzaa, B.J. O'Roak, M. Beddaoui, D. Alcantara, R.L. Conway, J. St-Onge, J.A. Schwartzentruber, K.W. Gripp, S.M. Nikkel, et al. Finding of Rare Disease Genes (FORGE) Canada Consortium. 2012. De novo germline and postzygotic mutations in AKT3, PIK3R2 and PIK3CA cause a spectrum of related megalencephaly syndromes. *Nat. Genet.* 44:934–940. https://doi.org/10.1038/ng.2331

Rodriguez-Laguna, L., K. Ibañez, G. Gordo, S. Garcia-Minaur, F. Santos-Simarro, N. Agra, E. Vallespín, V.E. Fernández-Montaño, R. Martín-Arenas, Á. Del Pozo, et al. 2018. CLAPO syndrome: identification of somatic activating PIK3CA mutations and delineation of the natural history and phenotype. *Genet. Med.* 20:882–889. https://doi.org/10.1038/gim.2017.200

Sabine, A., Y. Agalarov, H. Maby-El Hajjami, M. Jaquet, R. Hägerling, C. Pollmann, D. Bebber, A. Pfenniger, N. Miura, O. Dormond, et al. 2012. Mechanotransduction, PROX1, and FOXC2 cooperate to control connexin37 and calcineurin during lymphatic-valve formation. *Dev. Cell.* 22:430–445. https://doi.org/10.1016/j.devcel.2011.12.020

Srinivasan, R.S., M.E. Dillard, O.V. Lagutin, F.J. Lin, S. Tsai, M.J. Tsai, I.M. Samokhvalov, and G. Oliver. 2007. Lineage tracing demonstrates the venous origin of the mammalian lymphatic vasculature. *Genes Dev.* 21:2422–2432. https://doi.org/10.1101/gad.1588407

Timke, C., M.F. Krause, H.C. Oppermann, I. Leuschner, and A. Claviez. 2007. Interferon alpha 2b treatment in an eleven-year-old boy with disseminated lymphangiomatosis. *Pediatr. Blood Cancer.* 48:108–111. https://doi.org/10.1002/pbc.20461

Trenor, C.C. III, and G. Chaudry. 2014. Complex lymphatic anomalies. *Semin. Pediatr. Surg.* 23:186–190. https://doi.org/10.1053/j.sempedsurg.2014.07.006

Triana, P., M. Dore, V.N. Cerezo, M. Cervantes, A.V. Sanchez, M.M. Ferrero, M.D. Gonzalez, and J.C. Lopez-Gutierrez. 2017. Sirolimus in the Treatment of Vascular Anomalies. *Eur. J. Pediatr. Surg.* 27:86–90.

Truman, L.A., K.L. Bentley, E.C. Smith, S.A. Massaro, D.G. Gonzalez, A.M. Haberman, M. Hill, D. Jones, W. Min, D.S. Krause, and N.H. Ruddle. 2012. ProxTom lymphatic vessel reporter mice reveal Prox1 expression in the adrenal medulla, megakaryocytes, and platelets. *Am. J. Pathol.* 180:1715–1725. https://doi.org/10.1016/j.ajpath.2011.12.026

Wang, J., G. Kilic, M. Aydin, Z. Burke, G. Oliver, and B. Sosa-Pineda. 2005. Prox1 activity controls pancreas morphogenesis and participates in the production of "secondary transition" pancreatic endocrine cells. *Dev. Biol.* 286:182–194. https://doi.org/10.1016/j.ydbio.2005.07.021

Wang, W., H. Wang, X. Zhou, X. Li, W. Sun, M. Dellinger, B.F. Boyce, and L. Xing. 2017. Lymphatic Endothelial Cells Produce M-CSF, Causing Massive Bone Loss in Mice. *J. Bone Miner. Res.* 32:939–950. https://doi.org/10.1002/jbmr.3077

Yeager, N.D., S. Hammond, J. Mahan, J.T. Davis, and B. Adler. 2008. Unique diagnostic features and successful management of a patient with disseminated lymphangiomatosis and chylothorax. *J. Pediatr. Hematol. Oncol.* 30:66–69. https://doi.org/10.1097/MPH.0b013e318159a55a